

Magnetocaloric properties of melt-extracted $Gd_{87.5}Co_{12.5}$ crystalline/crystalline composite microwires

Chenzhi Li(李晨志), Zheng Wu(吴征), Yuhai Qu(瞿玉海), Yuxian Cao(曹昱宪), Xianda Liu(刘贤达), Wei Yi(易伟), Wenyi Peng(彭文屹)

Citation: Chin. Phys. B. 35, 097503 (2026). DOI: 10.1088/1674-1056/ae3f93 | CSTR: 32038.14.CPB.ae3f93

http://cpb.iphy.ac.cn; http://iopscience.iop.org/cpb

What follows is a list of articles you may be interested in

Enhanced low-field magnetocaloric effect induced by Co doping in $RCu_{2-x}Co_x$ (R = Er, Ho) compounds for liquid hydrogen

Lu Tian(田路), Zhaojun Mo(莫兆军), Xuanyu Qiao(乔轩雨), Chenyang Ma(马辰洋), Guodong Liu(刘国栋)

Chin. Phys. B. 35, 077505 (2026). DOI: 10.1088/1674-1056/ae360a | CSTR: 32038.14.CPB.ae360a

Heat recycling with magnetocaloric materials for sustainable energy conversion

Fengqi Zhang(张烽起), Yang Ren(任洋)

Chin. Phys. B. 35, 077502 (2026). DOI: 10.1088/1674-1056/ae3693 | CSTR: 32038.14.CPB.ae3693

Review of the strategies for regulating working temperatures of rare-earth-based low temperature magnetic cooling materials

Jie Zhao(赵洁), Yawei Gao(高亚伟), Dingsong Wang(王鼎淞), Shuxian Yang(杨淑娴), Lei Xi(奚磊), Hao Liu(刘昊), Yang Pan(潘洋), Jiawang Xu(许家旺), Xinqi Zheng(郑新奇), Shouguo Wang(王守国)

Chin. Phys. B. 35, 077501 (2026). DOI: 10.1088/1674-1056/ae3f92 | CSTR: 32038.14.CPB.ae3f92

Strain energy enhanced room-temperature magnetocaloric effect in Mn_5Ge_3

Xiaohe Liu(刘潇贺), Ping Song(宋平), Sen Yao(姚森), Yuhao Lei(雷雨豪), Ling Yang(杨玲), Shenxiang Du(杜深祥), Yiran Deng(邓贻然), Defeng Guo(郭得峰)

Chin. Phys. B. 35, 027505 (2026). DOI: 10.1088/1674-1056/adf6a6 | CSTR: 32038.14.CPB.adf6a6

Tuning the magnetocaloric and structural properties of $La_{0.67}Sr_{0.28}Pr_{0.05}Mn_{1-x}Co_xO_3$ refrigeration materials

Changji Xu(徐长吉), Xinyu Jiang(姜心雨), Zhengguang Zou(邹正光), Zhuojia Xie(谢卓家), Weijian Zhang(张伟建), Min Feng(冯敏)

Chin. Phys. B. 33, 127501 (2024). DOI: 10.1088/1674-1056/ad8550

Magnetocaloric properties of melt-extracted $Gd_{87.5}Co_{12.5}$ crystalline/crystalline composite microwires

Chenzhi Li(李晨志)[1,†], Zheng Wu(吴征)[1,†], Yuhai Qu(瞿玉海)[1,2,‡], Yuxian Cao(曹昱宪)[3], Xianda Liu(刘贤达)[1], Wei Yi(易伟)[4], and Wenyi Peng(彭文屹)[1]

[1] *School of Physics and Materials Science, Nanchang University, Nanchang* 330031, *China*
[2] *Chongqing Research Institute of Nanchang University, Chongqing* 402660, *China*
[3] *Institute for Special Steel Research, Central Iron and Steel Research Institute, Beijing* 100081, *China*
[4] *International Institute for Materials Innovation, Nanchang University, Nanchang* 330031, *China*

(Received 16 December 2025; revised manuscript received 24 January 2026; accepted manuscript online 30 January 2026)

Gadolinium (Gd) is the benchmark magnetocaloric material, yet its performance requires optimization in terms of working temperature range, refrigeration capacity (RC) and heat exchange capacity. Here, we address this challenge through a synergistic strategy combining Co alloying (to create an *in-situ* dual-phase magnetocaloric system) and the melt-extraction technique (to directly shape the alloy into microwires). This approach fabricates $Gd_{87.5}Co_{12.5}$ (at.%) crystalline/ crystalline composite microwires. The resulting microstructure comprises a Gd-rich matrix embedded with a magnetocaloric Gd_3Co phase, both of which are crystalline. This dual-phase architecture yields a remarkable magnetic entropy change ($-\Delta S_m$) profile, which delivers an ultra-broad effective temperature span (δT) of 218.5 K (defined between the outer half-maximum points of the dual-peak magnetic entropy change vs. temperature curve, 107.6–326.1 K) and a high RC of 658.7 J/kg under 5 T. To our knowledge, this work represents the first investigation of the magnetocaloric effect (MCE) in Gd-based crystalline/crystalline composite microwires. More importantly, it validates a dual-route design paradigm: phase-composition engineering for broadened δT and RC, coupled with morphology engineering via melt-extraction for enhanced heat exchange. This work establishes a new paradigm for designing next-generation magnetocaloric materials with integrated performance enhancements, particularly for efficient magnetic refrigeration in applications like gas liquefaction.

Keywords: magnetocaloric effect, magnetic refrigeration, melt extraction

PACS: 75.30.Sg, 07.20.Mc, 81.10.Fq

DOI: 10.1088/1674-1056/ae3f93 **CSTR:** 32038.14.CPB.ae3f93

1. Introduction

Magnetic refrigeration (MR) based on the magnetocaloric effect (MCE) is an efficient and eco-friendly alternative to conventional vapor-compression systems, with potential applications ranging from household cooling to gas liquefaction.[1–3] The performance of an MR system relies on the magnetocaloric material, which cyclically absorbs and releases heat during magnetization and demagnetization cycles.[4] For practical application, high-performance magnetocaloric materials must meet several criteria:[5–7] (i) high refrigeration capacity (RC) to ensure effective heat transfer; (ii) a wide and continuous working temperature span (δT), critical for processes like gas liquefaction; (iii) effective heat exchange for compact device design; (iv) a cost-effective fabrication process.

To date, materials exhibiting a first-order magnetic phase transition (FOMPT) have attracted considerable attention due to their large magnetic entropy change (ΔS_m), including Gd–Ge–Si,[8] Mn–Fe–P–Si,[9] and La–Fe–Si-based alloys.[10] However, their practical application is hampered by thermal hysteresis and a narrow operating temperature range. In contrast, materials with a second-order magnetic phase transition (SOMPT) exhibit a fully reversible MCE with negligible hysteresis.[5] Although their peak ΔS_m is lower, they can achieve a higher net RC owing to a broader δT and the absence of hysteresis.[11] Among magnetocaloric materials with SOMPT, Gd is considered the benchmark refrigerant due to its negligible thermal and magnetic hysteresis, a reproducible MCE over extended cycling, a wide working temperature range, and a large RC.[12,13] Nevertheless, developing materials that surpass pure Gd's performance, especially in terms of δT and heat exchange capability, remains a critical challenge for advancing MR technology.

To optimize Gd-based materials, researchers have explored alloying with elements like Co, Sc, or Zr to form solid solutions or multiphase microstructures, boosting RC.[14–16] However, bulk geometries suffer from low surface-area-to-volume ratios, severely limiting heat exchange with refrigerant fluids.[17] Additionally, achieving chemical homogeneity in bulk alloys often requires prolonged post-annealing,[14–16] increasing production costs and risking microstructural degradation (e.g., grain coarsening, surface oxidation). While Gd

[†]These authors contributed equally to this work.
[‡]Corresponding author. E-mail: yhqu@ncu.edu.cn

© 2026 Chinese Physical Society and IOP Publishing Ltd. All rights, including for text and data mining, AI training, and similar technologies, are reserved.

wires fabricated via cold rolling/drawing improve heat exchange, they exhibit reduced $-\Delta S_m$ and a narrowed δT unless annealed, which adds costs.[13] Thus, existing methods fail to make Gd-based crystalline alloys concurrently meet all four criteria for high-performance magnetocaloric materials.

To overcome these intertwined limitations, a synergistic approach is needed. Recent studies suggest that designing *in-situ* multiple-phase systems comprising multiple magnetocaloric phases can achieve a wide working temperature range by superimposing multiple transitions.[16,18,19] The Gd–Co system, particularly near the Gd-rich composition, is a prototypical example of such an *in-situ* dual-phase magnetocaloric material.[16] It naturally solidifies into a mixture of a ferromagnetic Gd-rich matrix (Curie temperature, $T_c \approx 294$ K) and an antiferromagnetic Gd_3Co phase (Néel temperature, $T_N \approx 134$ K). This unique dual-phase configuration results in a dual-peak-bridged broad plateau in the $-\Delta S_m$ profile over a broad temperature range, which is highly desirable for magnetic refrigeration applications. Concurrently, the melt-extraction technique enables one-step fabrication of continuous microwires with favorable heat exchange geometry, while shortening the annealing duration required for phase homogeneity compared to conventional arc melting.[9,20] Therefore, the combined approach of Co addition and melt extraction is expected to produce Gd–Co crystalline/crystalline composite microwires that require no annealing, exhibit a high specific surface area, a broad refrigeration temperature window, and a large effective RC. However, this possibility has not yet been explored.

Building on these insights, we fabricated $Gd_{87.5}Co_{12.5}$ crystalline/crystalline composite microwires via a single-step melt-extraction process, eliminating the need for post-annealing. The selection of this specific composition ($Gd_{87.5}Co_{12.5}$) is motivated by two key considerations: (i) According to the Gd–Co binary phase diagram,[21] this composition lies within the two-phase coexistence region of Gd (hcp) and Gd_3Co (orthorhombic), ensuring the formation of the desired dual-phase structure; (ii) The distinct magnetic transitions of the Gd matrix (ferromagnetic–paramagnetic, FM–PM, ~ 294 K) and the Gd_3Co phase (antiferromagnetic–paramagnetic, AFM–PM, ~ 134 K) are expected to superimpose, resulting in a broad plateau-like magnetic entropy change profile and an extended operating temperature window. Through comprehensive microstructural, magnetic, and magnetocaloric characterization, we demonstrate that these microwires simultaneously achieve an ultra-broad effective working temperature span (δT) of 218.5 K (evaluated between the outer half-maxima of the dual $-\Delta S_m$ peaks), a high RC of 658.7 J/kg under 5 T, and a microwire geometry optimized for heat exchange. This work establishes a new paradigm for designing next-generation magnetocaloric materials with enhanced integrated performance, particularly for gas liquefaction applications.

2. Experimental details

A master ingot with a nominal composition of $Gd_{87.5}Co_{12.5}$ (at.%) was prepared by arc-melting high-purity Gd (99.99%) and Co (99.99%) under a high-purity argon atmosphere. The ingot was flipped and remelted at least five times to ensure chemical homogeneity. Continuous microwires were directly fabricated from this ingot using the single-roller melt-extraction technique. The extraction chamber was first evacuated and then back-filled with argon gas to prevent oxidation. The ingot was inductively melted in a boron nitride (BN) crucible. Once a homogeneous molten state was achieved, the melt was elevated until it made contact with the edge of a rapidly rotating molybdenum (Mo) disk (surface velocity corresponding to ~ 3500 rpm). The molten metal was instantly drawn and solidified into continuous wires, which were then ejected and collected.

The phase structure of the as-prepared microwires was characterized by x-ray diffraction (XRD, Bruker D8 Advance) with Cu K_α radiation ($\lambda = 0.15406$ nm), recorded at a scan rate of 1 °/min. The general microstructure, phase distribution, and chemical composition were characterized by scanning electron microscopy (SEM, Zeiss Gemini 500) equipped with an energy-dispersive x-ray spectroscopy (EDS) detector. Back-scattered electron (BSE) imaging mode was primarily used to provide atomic number contrast. Transmission electron microscopy (TEM) and selected-area electron diffraction (SAED) were further employed to unambiguously identify the crystal structure and distribution of the constituent phases.

Magnetic properties were measured using a vibrating sample magnetometer (VSM) on a physical property measurement system (PPMS, Quantum Design). Isothermal magnetization curves were collected over a temperature range of 40–390 K.

3. Results and discussion

Figure 1(a) shows the digital photograph of the as-prepared melt-extracted $Gd_{87.5}Co_{12.5}$ microwires, which exhibit a loose, fluffy bulk morphology composed of numerous randomly entangled, fine filaments with diameters on the micrometer scale. This macroscopic appearance directly reflects the continuous, high-rate solidification characteristic of the melt-extraction process, which enables the large-scale production of uniform, high-aspect-ratio microwires. Figure 1(b) presents the XRD pattern of the as-prepared melt-extracted microwires. From Fig. 1(b), it can be seen that the diffraction peaks can be unequivocally indexed to the hexagonal close-packed (hcp) Gd phase (space group: $P6_3/mmc$)[16,22,23] and the orthorhombic Gd_3Co phase (space group: *Pnma*).[16,23]

The lattice parameters for these phases were calculated from the prominent diffraction peak positions using Bragg's law ($2d\sin\theta = \lambda$) and the corresponding plane-spacing formulas for each crystal system. For the hcp Gd phase, the a and c parameters were directly derived from the $(10\bar{1}0)$ and (0002) reflections, yielding values of $a = b = 0.3624$ nm and $c = 0.5810$ nm. For the orthorhombic Gd_3Co phase, a set of linear equations based on the (201), (401), and (220) reflections was solved to obtain $a = 0.7058$ nm, $b = 0.9536$ nm, and $c = 0.6331$ nm. This approach ensured high accuracy without the need for multi-peak fitting. The calculated values are in close agreement with literature data.[16,22,23] Figure 1(c) displays a refined and uniform microstructure consisting of well-defined dendritic morphology. Quantitative EDS point analysis (Table 1) confirms that the dark-contrast matrix is a Gd-rich phase with a mean composition of 98.5 at.% Gd and 1.5 at.% Co, while the bright interdendritic regions exhibit a near-stoichiometric Gd_3Co composition, averaging 75.4 at.% Gd and 24.6 at.% Co. The low standard deviation in the EDS measurements across multiple points further reflects the high chemical homogeneity of both phases. Using ImageJ software, the volume fractions of the Gd and Gd_3Co phases in the as-prepared $Gd_{87.5}Co_{12.5}$ microwires were determined to be 60.5 vol.% and 39.5 vol.%, respectively.

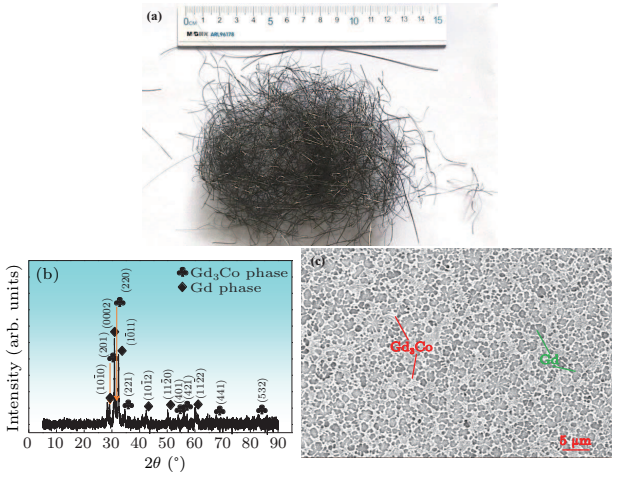


Fig. 1. Macro morphology, phase and microstructure of melt-extracted $Gd_{87.5}Co_{12.5}$ alloy microwires. (a) Digital photograph showing the macroscopic morphology of the as-prepared microwires; (b) XRD pattern showing the dual-phase structure of hcp Gd and orthorhombic Gd_3Co; (c) BSE micrograph revealing a uniform dendritic morphology, with a Gd-rich matrix (dark contrast) and a Gd_3Co interdendritic phase (bright contrast).

To further unambiguously determine the crystal structure of the constituent phases, TEM analysis was performed, and the results are presented in Fig. 2. The bright-field image in Fig. 2(a) clearly reveals the distribution of the two phases in the melt-extracted $Gd_{87.5}Co_{12.5}$ alloy microwire. From the corresponding SAED patterns, the bright phase (see the green dashed frame) and the dark phase (see the red dashed frame) were identified as the Gd and Gd_3Co phases, respectively. To further confirm the identification of both phases in the melt-extracted $Gd_{87.5}Co_{12.5}$ alloy microwire, TEM-EDS point analysis was carried out, and the results are also listed in Table 1. From Table 1, it can be seen that the Gd phase contains 97.48 at.% Gd and 2.53 at.% Co, while the Gd_3Co phase consists of 74.88 at.% Gd and 25.12 at.% Co. These results are consistent with the SEM-EDS data, providing strong corroboration for the existence of the Gd-rich matrix and the Gd_3Co phase. Figure 2(b) shows the TEM-EDS elemental maps. As shown in Fig. 2(b), the Gd signal appears nearly uniform across the microstructure due to the high Gd atomic fraction in both phases, resulting in weak compositional contrast. In contrast, the Co map exhibits a sharp concentration gradient, ranging from $\sim$ 2.53 at.% in the matrix to $\sim$ 25.12 at.% in the interdendritic phase, which unambiguously delineates the phase distribution. The distinctive architecture of a Gd-rich matrix hosting a fine, interconnected Gd_3Co phase is particularly advantageous: the ductile Gd-rich matrix ensures robust mechanical integrity, while the uniform and fine-scale distribution of both phases provides short and efficient diffusion paths. The combination of XRD, SEM, and TEM analyses confirms that the melt-extraction technique successfully enables the formation of the desired dual-phase structure in the $Gd_{87.5}Co_{12.5}$ microwires. Notably, this phase constitution ($Gd + Gd_3Co$) is consistent with the equilibrium phase diagram of the Gd–Co binary system,[21] indicating that the rapid solidification process retained the stable phases despite the high cooling rate.

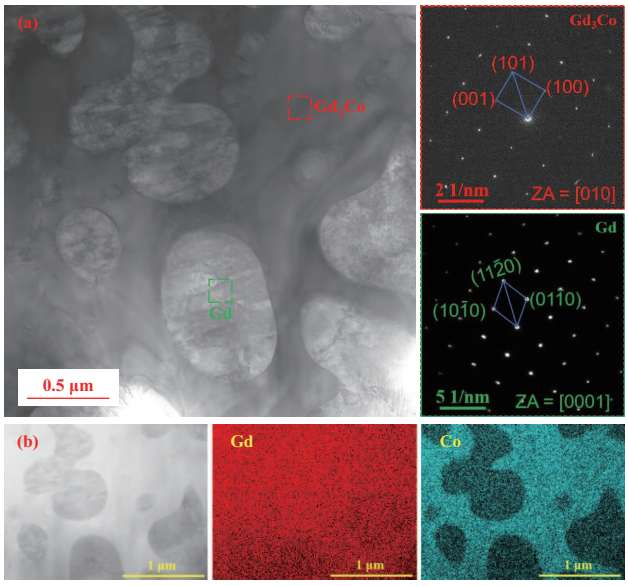


Fig. 2. TEM and TEM-EDS of melt-extracted $Gd_{87.5}Co_{12.5}$ alloy microwires. (a) TEM bright-field image and SAED patterns. (b) TEM-EDS elemental maps.

Figure 3(a) shows the temperature dependence of magnetization, $M(T)$, for the $Gd_{87.5}Co_{12.5}$ microwires measured under an applied field of 0.05 T. The zero-field-cooled (ZFC) curve was obtained by cooling the sample from 390 K to 5 K in zero field and subsequently measuring during warming under 0.05 T. The field-cooled (FC) curve was measured

during cooling under the same constant field. The inset displays the derivative, dM/dT, of the FC curve, revealing two distinct peaks at approximately 134 K and 294 K. According to previous studies,[12,13] pure Gd undergoes a ferromagnetic transition at $\sim$ 293 K. At the same time, the Gd_3Co compound undergoes an antiferromagnetic transition at $\sim$ 130 K.[16,24] Indeed, studies show that the transition temperatures of these phases are highly dependent on stoichiometry and vacancies.[13,14,16,25] Thus, the FM to PM transition at $\sim$ 294 K originates from the Gd matrix, while the AFM to PM transition at $\sim$ 134 K arises from the Gd_3Co phase. The close agreement of these transition temperatures with those reported for the bulk arc-melted alloy[16] indicates that the rapid solidification process inherent to melt extraction preserves the fundamental magnetic characteristics of the constituent phases. From Fig. 3(a), it can also be found that the ZFC and FC magnetization curves exhibit a distinct splitting below a characteristic irreversibility temperature (T_{irr}), which is indicative of spin-glass-like freezing behavior. In highly disordered magnetic systems, this effect is frequently observed and arises primarily from domain-wall pinning and the prominent magnetic anisotropy of the RE ions.[26] Figure 3(b) exhibits the $M(T)$ curves under 0.05 T in the field-cooled (FC) mode. The field-cooled magnetization in Fig. 3(b) demonstrates a composite magnetic system that undergoes dual second-order phase transitions. The most notable feature is the complete lack of thermal hysteresis between the cooling and heating branches, confirming the thermodynamic reversibility of the overall magnetic transformation process. This macroscopic reversibility implies that the separate phase transitions of the Gd and Gd_3Co phases are individually reversible. Thus, the broad and smoothly varying $M(T)$ curve is not an artifact of kinetic hindrance, but rather a direct result of the superposition of two reversible transitions occurring at different temperatures. The broadening of the phase transition originates from the material's microstructural features rather than compositional inhomogeneity within a single-phase alloy. This results in a system that combines high reversibility with a broad working temperature window, rendering it particularly promising for magnetocaloric applications.

Table 1. Quantitative EDS point analysis of the constituent phases in melt-extracted $Gd_{87.5}Co_{12.5}$ alloy microwires, showing excellent agreement between SEM-EDS and TEM-EDS despite the contrast reversal between the two techniques.

Technique	Phase & contrast	Element (at.%)	Point 1	Point 2	Point 3	Average
SEM-EDS	Gd-rich phase (dark)	Gd	98.1	98.9	98.5	98.5
		Co	1.9	1.1	1.5	1.5
	Gd_3Co phase (bright)	Gd	76.3	74.6	75.4	75.4
		Co	23.7	25.4	24.6	24.6
TEM-EDS	Gd-rich phase (bright)	Gd	98.73	94.85	98.87	97.48
		Co	1.27	5.18	1.13	2.53
	Gd_3Co phase (dark)	Gd	74.36	75.34	74.93	74.88
		Co	25.64	24.64	25.07	25.12

To further ascertain the reversibility of the phase transitions and to quantitatively evaluate the magnetocaloric performance, the isothermal magnetization curves ($M(H)$ curves) of the $Gd_{87.5}Co_{12.5}$ microwires were measured over a temperature range of 40–390 K. For clarity, the results are presented in two separate panels: Fig. 4(a) displays the $M(H)$ curves from 40 K to 210 K, encompassing the temperature range of the Gd_3Co phase transition, while Fig. 4(b) shows the curves from 220 K to 390 K, covering the transition of the Gd-rich matrix. As shown in Figs. 4(a) and 4(b), the $M(H)$ curves collected during the increasing and decreasing field cycles are nearly superimposed at every measured temperature. This absence of hysteresis in the $M(H)$ loops provides direct and compelling evidence for a highly reversible magnetization process, which is a critical prerequisite for efficient magnetocaloric applications with low hysteretic energy loss. The evolution of these isotherms, viewed across Figs. 4(a) and 4(b), delineates the magnetic behavior of the dual-phase system. In the low-temperature regime (Fig. 4(a), 40–130 K), the curves exhibit a rapid approach to technical saturation, characteristic of the coexisting ferromagnetic (Gd-rich) and canted antiferromagnetic (Gd_3Co) phases. As the temperature increases beyond the Néel temperature of the Gd_3Co phase ($T_N \approx 134$ K) and into the range shown in Fig. 4(b), the system enters a regime dominated by the ferromagnetic Gd matrix. Finally, above the Curie temperature of the Gd matrix ($T_c \approx 294$ K), the isotherms in Fig. 4(b) transition into linear, non-saturating curves, confirming the paramagnetic state of both phases. To rigorously determine the order of these magnetic transitions, Arrott plots (M^2 vs. $\mu_0 H/M$) of $Gd_{87.5}Co_{12.5}$ microwires were constructed from the isothermal magnetization data, as displayed in Figs. 4(c) and 4(d), corresponding to the same temperature ranges as Figs. 4(a) and 4(b), respectively. According to the Banerjee criterion,[27] a first-order magnetic phase transition is characterized by a negative slope in the Arrott plot, whereas a second-order transition exhibits a positive slope. As shown in Figs. 4(c) and 4(d), the Arrott plots across the entire temperature range, spanning both the T_N of the Gd_3Co phase and the T_c of the Gd matrix, show no negative slopes or inflection points. This provides definitive evidence for second-order

phase transitions, which is fully consistent with the absence of hysteresis observed in the $M(T)$ and $M(H)$ measurements (Figs. 3(b), 4(a), and 4(b)).

From the measured $M(H)$ curves, we determined the magnetic entropy change $(-\Delta S_{\rm m})$ as a function of temperature and magnetic field, employing the Maxwell relation for the calculation[26]

$$-\Delta S_{\rm m}(T,\Delta H) = S_{\rm m}(T,H) - S_{\rm m}(T,0) = \int_0^H \left(\frac{\partial M(H,T)}{\partial T}\right)_H {\rm d}H, \quad (1)$$

where M, H, and T denote the magnetization, the applied magnetic field and the temperature, respectively.

The $-\Delta S_{\rm m}$ at various external applied magnetic fields and temperatures for the melt-extracted $Gd_{87.5}Co_{12.5}$ dual-phase alloy microwires were assessed using Eq. (1) and are shown in Fig. 5. From Fig. 5, it can be found that the $-\Delta S_{\rm m}(T)$ for a magnetic field change of 0–5 T presents a distinct double-peak feature. Specifically, two well-resolved peaks are observed in the $-\Delta S_{\rm m}(T)$ curve, corresponding to the magnetic transitions of the two crystalline phases in the composite: the lower-temperature peak at $\sim$ 135 K arises from the antiferromagnetic–paramagnetic transition of the crystalline

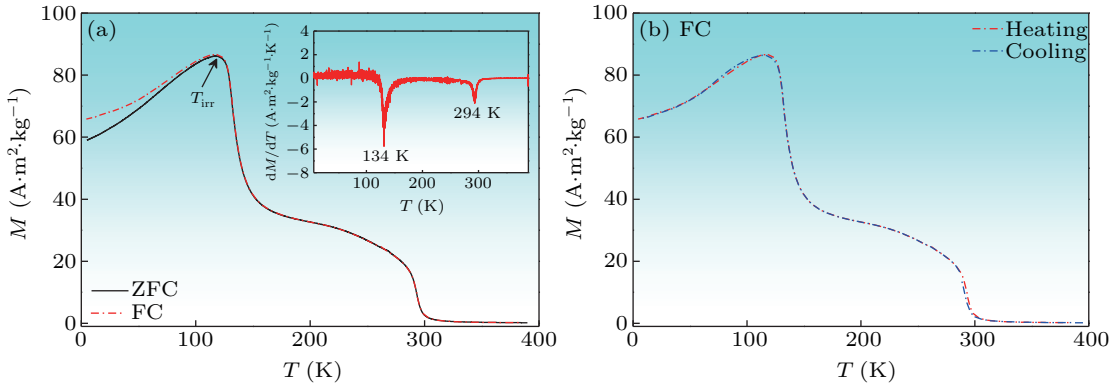


Fig. 3. (a) Temperature dependence of magnetization ($M(T)$) for melt-extracted $Gd_{87.5}Co_{12.5}$ alloy microwires under a magnetic field of 0.05 T in zero-field-cooled (ZFC) and field-cooled (FC) modes. The inset shows the derivative dM/dT of the FC curve. (b) The $M(T)$ curves in the field-cooled (FC) mode.

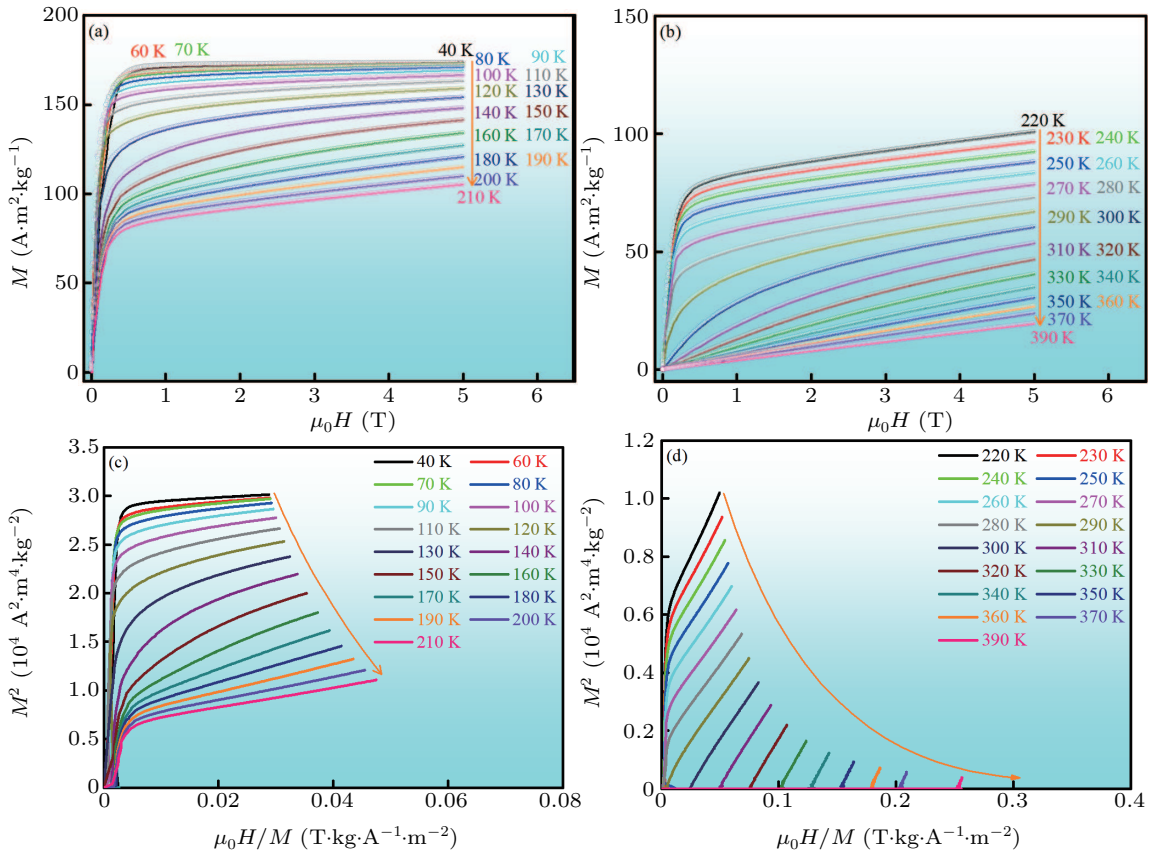


Fig. 4. $M(H)$ curves and Arrott plots of melt-extracted $Gd_{87.5}Co_{12.5}$ microwires. (a) $M(H)$ curves measured from 40 to 210 K. (b) $M(H)$ curves measured from 220 to 390 K. In panels (a) and (b), solid and short-dashed lines represent data measured under increasing and decreasing magnetic fields, respectively. (c) and (d) Corresponding Arrott plots (M^2 vs. $\mu_0 H/M$) derived from panels (a) and (b), respectively.

Gd_3Co phase, while the higher-temperature peak at $\sim$ 295 K originates from the ferromagnetic–paramagnetic transition of the crystalline Gd-rich matrix. This assignment is directly supported by the corresponding features in the $M(T)$ curves (Fig. 3) and the second-order transition behavior confirmed by the Arrott plots (Figs. 4(c) and 4(d)), collectively affirming the crystalline/crystalline composite nature of the microwires. Notably, these two transition peaks are bridged by a broad, relatively flat plateau, which enables an extended effective operating temperature range for magnetocaloric applications. The $-\Delta S_m(T)$ curve under 5 T spans a remarkably broad temperature interval of 218.5 K (from 107.6 K to 326.1 K), within which a substantial magnetocaloric effect is maintained. To quantify the effective operating temperature breadth, a key criterion for applications requiring continuous cooling, we evaluate the working temperature span (δT). For our dual-peak system, and in line with the reporting convention for composite magnetocaloric materials,[16,28] δT is defined as the temperature interval between the outer half-maximum points of the two peaks in the $-\Delta S_m(T)$ curve. Under a magnetic field change of 5 T, this δT reaches 218.5 K, extending from 107.6 K to 326.1 K. It is important to note that this definition captures the full continuous window over which a substantial magnetocaloric effect is maintained. Although the magnetic entropy change in the valley between the peaks is lower ($\sim$ 1.8 $J{\cdot}kg^{-1}\cdot K^{-1}$ under 5 T) compared to the peak values ($\sim$ 4.8 $J{\cdot}kg^{-1}\cdot K^{-1}$), it remains functionally significant and contributes to the overall refrigerant capacity. Consequently, this large δT value far exceeds the single-peak full-width at half-maximum of benchmark pure Gd ($\delta T \approx 70.0$ K),[29] highlighting the superior capability of our dual-phase system for wide-temperature-range applications such as gas liquefaction.

Beyond a high magnitude of entropy change ($|\Delta S_m|$), a large refrigeration capacity (RC) is essential for practical magnetocaloric applications. The RC, representing the amount of heat transferred between the hot and cold reservoirs in an ideal refrigeration cycle,[14,15] is quantified by integrating the area under the $|\Delta S_m(T)|$ curve over the full-width at half-maximum temperature span, calculated as follows:[16,19]

$$\mathrm{RC} = \int_{T_2}^{T_1} |\Delta S_m| \mathrm{d}T, \tag{2}$$

where T_1 and T_2 denote the temperatures that correspond to the half-maximum values on the two sides of the $\Delta S_m(T)$ curve, respectively. Using Eq. (2), the refrigeration capacity (RC) of the melt-extracted $Gd_{87.5}Co_{12.5}$ alloy microwires was calculated to be 658.7 J/kg, which is slightly lower than the value of 720.9 J/kg reported for its bulk arc-melted $Gd_{87.5}Co_{12.5}$ alloy.[16] This close agreement demonstrates that the rapid solidification inherent to the melt-extraction process successfully preserves the intrinsic magnetocaloric performance of the dual-phase $Gd_{87.5}Co_{12.5}$ alloy, despite the geometric shaping into microwires. More importantly, this RC value represents a substantial $\sim$ 52% enhancement over that of the benchmark material, pure Gd (RC $\approx$ 433.0 J/kg)[29] and is achieved over a dramatically broadened effective temperature window (218.5 K vs. $\sim$ 70.0 K for pure Gd). Evidently, the present microwires successfully address the key limitations of pure Gd by simultaneously achieving a high RC and an ultra-wide δT. It is worth noting that the definition of δT as the interval between the outer half-maximum points of the dual peaks is consistent with prior reports on dual-phase magnetocaloric materials,[16,28] providing a standardized metric for comparing the effective working temperature ranges of such systems.

The origin of the dual-peak-bridged broad plateau in the $-\Delta S_m$ profile of the melt-extracted $Gd_{87.5}Co_{12.5}$ alloy microwires can be attributed to the synergistic interplay between dual second-order magnetic phase transitions and the unique crystalline dual-phase architecture (see Fig. 1(b)). From a microstructural perspective, the dark Gd phase (60.5 vol.%) acts as the volume-dominant matrix phase in the alloy system, while it is segmented into dispersed regions by the continuously distributed Gd_3Co phase (39.5 vol.%). This structural configuration establishes two distinct magnetocaloric sources, with a large separation in their magnetic ordering temperatures ($T_N \approx 134$ K for Gd_3Co and $T_c \approx 294$ K for Gd) forming the structural basis for the wide operating window. Magnetically, the second-order nature of both transitions, confirmed by Arrott plots (Figs. 4(c) and 4(d)) and combined with negligible thermal and magnetic hysteresis (Figs. 3(b), 4(a), and 4(b)), facilitates a smooth superposition of their individual entropy changes.

To comprehensively evaluate the magnetocaloric performance of the melt-extracted $Gd_{87.5}Co_{12.5}$ alloy microwires, which constitute a fully crystalline/crystalline composite, their key parameters under 5 T are compared with those of other prominent Gd-based crystalline materials operating in similar temperature ranges, as summarized in Table 2. First, compared to typical crystalline alloys exhibiting a FOMPT, such as $Gd_5Si_{1.7}Ge_{2.3}$[8] and $Gd_5Si_2Ge_2$,[29] the present microwires demonstrate a broader working temperature range. Although FOMPT materials can achieve high peak magnetic entropy changes ($-\Delta S_m$), they suffer from significant hysteresis losses, which degrade refrigeration efficiency and device longevity. More critically, their useful magnetocaloric effect (MCE) is confined to a narrow temperature window ($\delta T \approx$ 19–28 K). In contrast, the dual SOMPT in our crystalline composite result in negligible hysteresis and an exceptional δT of 218.5 K, eliminating the need for complex composite strategies to broaden the temperature span. This clearly demonstrates an advantage in operational breadth and efficiency over FOMPT crystalline benchmarks. Second, in terms of performance breadth, these microwires outperform

other state-of-the-art Gd-based bulk crystalline materials with SOMPT. As shown in Table 2, typical SOMPT crystalline materials, such as $Gd_5Si_{1.7}Ge_{1.9}Fe_{0.4}$,[8] Gd_3Co,[25] pure Gd,[29] $Gd_5Si_2Ge_{1.9}Fe_{0.1}$,[30] and $Gd_6Co_2Si_3$,[31] while hysteresis-free, still exhibit limited δT values (typically $\leq$ 112 K) due to their single magnetic transition. By coupling the transitions of the Gd matrix and the Gd_3Co phase, our dual-phase microwires achieve a δT more than twice as wide while maintaining a competitive $-\Delta S_m$ peak and a high RC. This establishes the *in-situ* dual-crystalline-phase design as a superior strategy within the SOMPT family for achieving an exceptionally wide working temperature span. Third, the transition to a microwire geometry in this crystalline composite system represents a critical innovation. As the first report on the magnetocaloric effect of dual-phase crystalline Gd-based composite microwires, its performance merits direct comparison with its bulk crystalline counterpart. As indicated in Table 2, the developed $Gd_{87.5}Co_{12.5}$ microwires (RC = 658.7 J/kg) fully preserve the excellent table-like $-\Delta S_m$ profile and the majority of the RC inherent to the bulk crystalline $Gd_{87.5}Co_{12.5}$ alloy (RC = 720.9 J/kg),[16] confirming that rapid solidification effectively retains the intrinsic magnetocaloric properties of the crystalline phases. More importantly, the microwire morphology offers a potential solution to a key regenerator design challenge: heat exchange efficiency. Therefore, through the synergistic combination of a fully crystalline dual-phase composition, second-order transitions, and a microwire morphology, the present work advances the state-of-the-art in crystalline magnetocaloric materials by delivering a system that simultaneously excels in key performance metrics: ultra-wide δT, high RC, negligible hysteresis, and enhanced heat exchange potential, all via a scalable single-step process.

Table 2. Comparison of key magnetocaloric parameters for the $Gd_{87.5}Co_{12.5}$ microwire and other typical Gd-based crystalline materials under 5 T. (M) and (B) in parentheses represent the "microwire" and "bulk alloy", respectively. FOMPT and SOMPT denote first-order and second-order magnetic phase transitions. T_p denotes the peak temperature of the magnetic entropy change ($-\Delta S_m$).

Material	Transition type	$-\Delta S_m$ (J·kg^{-1}·K^{-1}) & T_p (K)	δT (K)	RC (J·kg^{-1})	Ref.
$Gd_{87.5}Co_{12.5}$ (M)	SOMPT	~ 4.8/134 K & 4.8/294 K	218.5[b]	658.7	this work
$Gd_5Si_{1.7}Ge_{2.3}$ (B)	FOMPT	17.5/240	19.7[a]	288.1	Ref. [8]
$Gd_5Si_{1.7}Ge_{1.9}Fe_{0.4}$ (B)	SOMPT	7.0/287 K	81.8[a]	455.6	Ref. [8]
$Gd_{87.5}Co_{12.5}$ (B)	SOMPT	~ 4.8/128 K & 4.2/293 K	236.7[b]	720.9	Ref. [16]
Gd_3Co (B)	SOMPT	11.1/129 K	42.8[a]	494.4	Ref. [25]
$Gd_5Si_2Ge_2$ (B)	FOMPT	19.0/270 K	28.0[a]	305.0	Ref. [29]
Pure Gd (B)	SOMPT	8.7/294 K	70.0[a]	433.0	Ref. [29]
$Gd_5Si_2Ge_{1.9}Fe_{0.1}$ (B)	SOMPT	7/305	64.0[a]	360.0	Ref. [30]
$Gd_6Co_2Si_3$ (B)	SOMPT	6.3/295 K	111.2[a]	503.0	Ref. [31]

[a]For materials with a single magnetic entropy change peak (e.g., pure Gd, Gd_3Co), δT reported is the conventional full width at half maximum.
[b]For dual-peak systems (this work and Ref. [16]), δT is defined as the temperature span between the outer half-maximum points of the two peaks.[16,28]

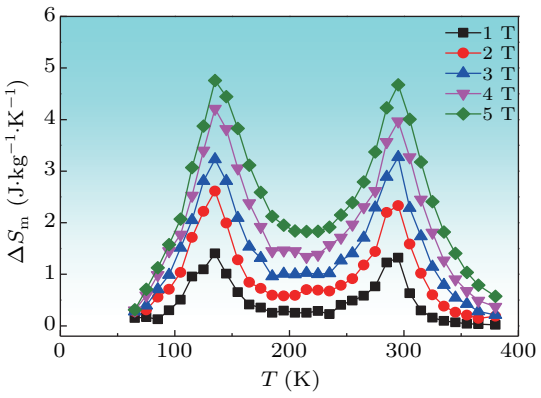


Fig. 5. Magnetic entropy change $-\Delta S_m$ as a function of temperature for melt-extracted $Gd_{87.5}Co_{12.5}$ microwires under different magnetic field changes.

While the *in-situ* dual-phase design successfully yields an ultra-broad effective temperature span (δT), the saddle-shaped inflection between the two peaks in the $-\Delta S_m$ profile (Fig. 5) indicates room for further optimization toward a more ideal table-like magnetocaloric response. It is noted that for the bulk counterpart of similar composition, merely varying the Gd/Co ratio to change the phase fractions has a limited effect on elevating the valley between the peaks.[16] This suggests that future optimization strategies should move beyond simple compositional tuning. Instead, focusing on enhancing the magnetic coupling between the two phases holds promise. The strong biphasic coupling observed in the bulk alloy, which broadens the magnetic transition,[16] implies that strengthening this interaction could promote a smoother superposition of the two magnetocaloric contributions. Potential pathways include interface engineering via post-processing (e.g., annealing) to improve interfacial coherency and elemental interdiffusion, which may intensify the exchange interaction at the FM/AFM interface. Additionally, the formation of an interconnected network of the Gd phase upon annealing, as reported to be crucial for mechanical enhancement,[16] might also facilitate magnetic interaction pathways across the microstructure. Applying such microstructural control to our melt-extracted microwires could be a fruitful direction to further flatten the $-\Delta S_m$ plateau, thereby optimizing the magnetocaloric performance for applications demanding a constant cooling power over a wide temperature range.

In conclusion, the $Gd_{87.5}Co_{12.5}$ alloy microwires fabricated via the melt-extraction technique uniquely integrate mul-

tiple advantages derived from their simple processing and material design: (i) hysteresis-free second-order transitions, (ii) a broad working temperature range enabled by the dual-phase design, (iii) high refrigeration capacity, (iv) a wire geometry optimized for heat exchange, and (v) a highly efficient and cost-effective manufacturing process due to single-step formation without the need for annealing. As the first demonstration of a Gd-based crystalline/crystalline composite magnetocaloric microwire, this work achieves a synergistic combination of straightforward fabrication, favorable material properties, and an advantageous geometry, establishing it as a highly promising candidate for next-generation magnetic refrigeration.

4. Conclusion

In summary, continuous $Gd_{87.5}Co_{12.5}$ crystalline/crystalline magnetocaloric microwires have been successfully fabricated via a one-step melt-extraction process without post-annealing. Microstructural characterization confirms the formation of an *in-situ* dual-phase composite consisting of a Gd-rich matrix embedded with a Gd_3Co phase. The microwires exhibit excellent magnetocaloric performance, combining a broad effective temperature span (δT, defined between the outer half-maxima of the dual peaks) of 218.5 K with a high refrigeration capacity of 658.7 J/kg under 5 T. This performance arises from the superposition of two reversible second-order magnetic transitions, which together maintain a functionally useful ΔS_m across the entire wide temperature window, despite a lower value in the valley region. This study demonstrates that the synergistic combination of an *in-situ* dual-phase design (via Co alloying) and the melt-extraction technique provides an effective dual-route strategy to simultaneously achieve an extended operating temperature range, high refrigeration capacity, and enhanced heat exchange capability in a single material system. The results establish Gd-based crystalline/crystalline composite microwires as a promising candidate for efficient magnetic refrigeration, particularly in applications such as gas liquefaction. The presented approach is also expected to be applicable to other rare-earth-based magnetocaloric systems.

Acknowledgments

Project supported by the National Natural Science Foundation of China (Grant Nos. 52301014 and 52363031), the Natural Science Foundation of Chongqing (Grant No. CSTB2022NSCQ-MSX0389), the Jiangxi Provincial Natural Science Foundation (Grant Nos. 20212BAB214052 and 20224BAB204012), the College Students' Innovative Entrepreneurial Training Plan Program (Grant Nos. 202310403025, 202410403090 and 202610403082), and the Open Sharing Fund for the Large Instruments and Equipments of Nanchang University (Grant No. 2024CX04). We acknowledge eceshi (www.eceshi.com) for the XRD characterization.

References

[1] Zhang Y K, Hao W X, Hu C L, Wang X, Zhang X F and Li L W 2023 *Adv. Funct. Mater.* **33** 2310047
[2] Liu W, Scheibel F, Gottschall T, Bykov E, Dirba I, Skokov K and Gutfleisch O 2021 *Appl. Phys. Lett.* **119** 022408
[3] Kumar S, Muhammed R, Kim S, Yi J, Son K and Oh H 2024 *Adv. Funct. Mater.* **34** 2402513
[4] Wang X J, Zong S T, Zhang Y, Mo Z J, Qiao J W and Liaw P K 2024 *Appl. Phys. Lett.* **124** 122412
[5] Li J T, Zhou J M, Peng W Y, Cao Y X, Wu Z, Ding Z Y and Qu Y H 2025 *Intermetallics* **186** 108955
[6] Aseguinolaza I R, Herrero A, Garcia-Adeva A J, Apiñaniz E, Garshev A V, Morozkin A V and Oleaga A 2025 *J. Alloys Compd.* **1010** 177154
[7] Wei S J, Shen H X, Zhang L Y, Cao F Y and Sun J F 2024 *J. Mater. Res. Technol.* **33** 6216
[8] Uthaman B, Raji G R, Thomas S, Suresh K G and Varma M R 2019 *Intermetallics* **115** 106629
[9] Luo L, Shen H X, Zhang L Y, Sun J F and Phan M H 2024 *J. Alloys Compd.* **1003** 175579
[10] Imaizumi K, Fujita A, Suzuki A, Kobashi M and Ozaki K 2022 *Acta Mater.* **227** 117726
[11] Ghosh S, Ghosh A and Mandal K 2018 *J. Alloys Compd.* **746** 200
[12] Yang W S, Kim J H, Kim M J, Yang S Y, Lee A Y, Esmaeilpoor H, Kim J H, Lee K S and Shin D S 2025 *J. Alloys Compd.* **1014** 178657
[13] Kim J H, Shin D S, Yoon J S and Lee K S 2022 *J. Mater. Res. Technol.* **21** 4636
[14] Zhong X C, Shen X Y and Liu Z W 2016 *J. Rare Earths* **34** 889
[15] Uporov S A and Sterkhov E V 2024 *Solid State Commun.* **380** 115444
[16] Zhong H, Song Y Z, Long F X, Lu H, Ai M J, Li T Y, Yao Y H, Sakai Y, Ikeda M, Takahashi K, Azuma M, Hu F X, Xing X R and Chen J 2024 *Adv. Mater.* **36** 2402046
[17] Guel-Rodríguez M, Zamora J, Sanchez-Valdés C F, Sánchez Llamazares J L and Álvarez-Alonso P 2024 *J. Alloys Compd.* **978** 173452
[18] Remya U D, Arun K, Swathi S, Athul S R, Andrea D, Marian R and Nagalakshmi R 2023 *J. Rare Earths* **41** 1721
[19] Wu X F, Du Y S, Gao X Q, Liu F, Ma L, Cheng G, Wang J, Zhao J T and Rao G H 2025 *J. Alloys Compd.* **1010** 177742
[20] Zhang H H, Qian M F, Zhang X X, Jiang S D, Wei L S, Xing D W, Sun J F and Gen L 2017 *Mater. Des.* **114** 1
[21] Wu Y, Wang J, Yao Q R, Chen Q, Rao G H and Zhou H Y 2025 *Trans. Mater. Res.* **1** 100060
[22] Saidi M, Walha S, Nouri K, Kabadou A, Bassais L and Jemmali M 2019 *J. Alloys Compd.* **792** 87
[23] Huang J L, Zhong H C, Xia X W, He W, Zhu J M, Deng J Q and Zhuang Y H 2009 *J. Alloys Compd.* **471** 74
[24] Burzo E 1972 *Phys. Rev. B* **6** 2882
[25] Mo Z J, Shen J, Yan L Q, Wu J F, Tang C C and Shen B G 2013 *J. Appl. Phys.* **113** 033908
[26] Zhang Y K, Ying J Y, Gao X Q, *et al.* 2023 *J. Mater. Sci. Technol.* **159** 163
[27] Banerjee B K 1964 *Phys. Lett.* **12** 16
[28] Feng J Q, Liu Y H, Sui J H, *et al.* 2021 *Mater. Today Phys.* **21** 100528
[29] Pecharsky V K and Gschneidner K A 1997 *Phys. Rev. Lett.* **78** 4494
[30] Provenzano V, Shapiro A J and Shull R D 2004 *Nature* **429** 853
[31] Shen J, Wu J F and Sun J R 2009 *J. Appl. Phys.* **106** 083902